

Microphone array wind tunnel measurements of Reynolds number effects in high-speed train aeroacoustics

Andreas Lauterbach, Klaus Ehrenfried, Sigfried Loose, and Claus Wagner

*German Aerospace Center (DLR), Institute of Aerodynamics and Flow Technology
Bunsenstrasse 10, 37073 Göttingen, Germany*

The present study focuses on the Reynolds number dependence of high-speed train aeroacoustic sound sources. To cover a wide range of Reynolds numbers the experimental investigations are carried out on a 1 : 25 scale-model of the high-speed train Inter City Express 3 by conducting microphone array measurements in two wind tunnels. The latter are the Aeroacoustic Wind tunnel (AWB) of the German Aerospace Center (DLR) in Brunswick, providing nearly perfect acoustical conditions, and the Cryogenic wind tunnel (DNW-KKK) of the DNW (German - Dutch wind tunnels) in Cologne, allowing measurements at higher Reynolds numbers. Two types of sound sources with different characteristics at Reynolds numbers of up to $Re = 0.46 \times 10^6$ have been identified by measurements in the AWB. It was found, that the aeroacoustic noise from the bogie section is dominant for frequencies $f < 5$ kHz and can be characterised by cavity mode excitation. Further, the pantograph is the dominant sound source above $f = 5$ kHz with an Aeolian tone characteristic. Additional aeroacoustic measurements have been conducted in the cryogenic wind tunnel DNW-KKK in order to analyse the Reynolds number dependence of the noise generated at the first bogie, for higher Reynolds numbers of up to $Re = 3.70 \times 10^6$. The DNW-KKK admits varying the Mach and Reynolds numbers independently. These measurements reveal only a weak Reynolds number dependence of the noise source generated at the first bogie.

1. INTRODUCTION

Modern high-speed trains allow for operational speeds of up to 350 km/h, which also means an increase of emitted sound. Based on measurements, Barsikow et al. [1] as well as Mellet et al. [2] propose a power exponent for the relation between train velocity and emitted sound powers for the wheel/rail interaction between $m = 3$ and $m = 4$. For the aerodynamic noise, Pfizenmaier et al. [3] predict an exponent of about $m = 6$, which corresponds to a typical aeroacoustic dipole. Fig. 1 depicts the relations between the sound power levels of different sound sources and the velocity of the train, according to Dittrich et al. [4]. It can be seen, that for train velocities higher than 220 km/h, aerodynamic noise exceeds all other sound sources, such as engine/gearbox noise, noise from aggregates, general noise related to the bogies and wheel/rail interaction. The aeroacoustic

plays a major role for the design of new high-speed trains. Therefore, for the desired reduction of aerodynamic noise, the detailed knowledge about the distribution and the properties of the sound sources is needed.

In the field of high-speed train acoustics, investigations have been done on the full-scale vehicles, as well as on scaled models in wind tunnels. Full-scale tests can provide comprehensive knowledge of the aeroacoustic properties of a train. The disadvantage is that these tests can be only performed when the train is already in operation, and so it is impossible to analyse acoustics during the design process. Most of the earlier publications in this field report on full-scale drive-by tests and focus on the so-called wheel-rail noise. Barsikow et al. [5] used a one-dimensional line array mounted along the wayside in two orientations to study this kind of sound source. Using their technique, they were able to separate

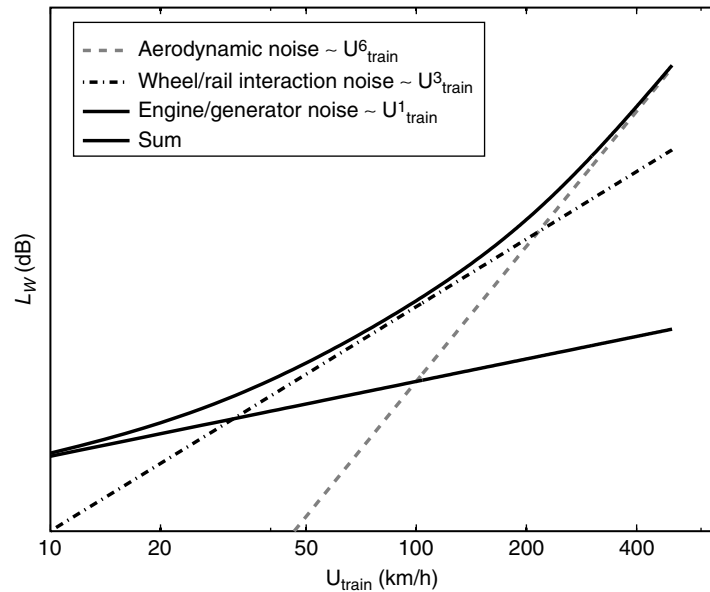


Figure 1: The relation between sound power levels of different sound sources and the train velocity, based on the work of Dittrich et al. [4].

wheel-rail noise from aeroacoustic sources. Modern microphone array techniques became more and more effective for the localisation of aeroacoustic sound sources. Martens et al. [6] present full-scale drive-by measurements conducted on an Inter City Express 3 (ICE 3), a high-speed train which is operational in Germany, and the ETR 500, an Italian high-speed train. They used a two-dimensional microphone array with 90 microphones. The large aperture of 4 m provides a good resolution of the sound sources of the trains. Wheel-rail noise as well as aeroacoustic sound sources, such as the pantograph, the bogie cavities, antennas and air inlets or outlets can be identified on the source maps. With the objective of predicting the aeroacoustic properties during the design process, Yamazaki et al. [7] investigated the aerodynamic noise of a simplified scale-model of a train in a wind tunnel at Reynolds numbers of up to 2×10^6 , also using the microphone array technique. Their more qualitative study focused on the noise generated at the bogie cavities and the gaps between the coaches. Based on these measurements, noise reduction measures were developed and applied to a full-scale train. Other wind tunnel

studies report on the aeroacoustic optimisation of parts of trains, e.g. the pantograph (see [8–11]). In spite of the interest of this subject, a comprehensive quantitative aeroacoustic study of trains in wind tunnels over a wide Reynolds number range, which includes the identification of the source mechanisms and their Mach and Reynolds number dependence, is still an open issue.

It would be extremely valuable to gain more knowledge on how aeroacoustic measurements conducted on scale-models in the wind tunnel, and full-scale tests compare with each other.

The purpose of the paper is to gain insight into the Reynolds - and Mach number effects of the sound sources of high-speed trains. To achieve this, experiments on two different aeroacoustic sources are performed: the pantograph and the noise emitted by the first bogie. It is shown that these two sources can be described by a cylinder in cross flow and by a certain kind of cavity mode excitation, respectively. These results are obtained by measurements in an aeroacoustic wind tunnel, described in Sec. 4.1, which provides nearly perfect acoustic conditions. The trade-off is its limitation in realising larger Reynolds

numbers. The Reynolds number scales with the scale of the wind tunnel model, as long as the Mach number and the physical properties of the fluid are not changed. With air as fluid at standard conditions, it is impossible to obtain the Reynolds number of a full-scale train, using a scale-model. In order to increase the Reynolds number, conducting the measurements in a cryogenic wind tunnel is an appropriate method (see Goodyer and Kilgore [12]). Furthermore, Reynolds and Mach number depending effects of aerodynamics can be investigated very satisfactory in such facilities, because both coefficients can be varied independently. Therefore, this paper reports in Sec. 4.2 on a second measurement campaign in a cryogenic wind tunnel. Effects of cooling down the fluid on aeroacoustics are discussed in the following Sec. 2.

2. SCALING CONCEPTS

The following two sections introduce into aerodynamic and aeroacoustic scaling. For both, the role of the temperature is discussed. The cryogenic conditions influence the aerodynamics as well as the aeroacoustics.

2.1. AERODYNAMIC SCALING

The Reynolds number is an important non dimensional parameter in the scope of aerodynamic scaling and can be seen as the ratio of inertia to viscous forces. This coefficient can describe the state of the flow:

$$Re = \frac{U_\infty \cdot L \cdot \rho}{\mu}. \quad (1)$$

U_∞ denotes the free stream velocity, ρ the density, L a characteristic length and μ the dynamic viscosity. Independent of the scale of the model, for a constant Reynolds number, one can expect the same flow topology, as long as the shape of the model is not changed. This holds true as long as

compressibility effects are not relevant, and the Mach number is small enough:

$$M = \frac{U_\infty}{c} < 0.3. \quad (2)$$

The speed of sound c is a function of the temperature T . For ideal gases the relation reads:

$$c(T) = \sqrt{\kappa \cdot R \cdot T}, \quad (3)$$

with the ideal gas constant R . The top graph in Fig. 2 depicts the relation between speed of sound and temperature in the temperature range of $100 \text{ K} < T < 300 \text{ K}$, the relevant range for the current experiments. The specific heats for diatomic gases $\kappa = 1.4$ can be seen as constant within this range; the relative deviations are less than 1.7 %. For more details see Hilsenrath et al. [15]. The density of the fluid is a function of temperature and pressure. The ideal gas law provides the relation between density, pressure and temperature:

$$\rho(T, p) = \frac{p}{R \cdot T}. \quad (4)$$

The relation for a constant pressure (this parameter has been kept constant during the experiments in the cryogenic wind tunnel) between temperature and density is shown in Fig. 2, the middle graph. The dynamic viscosity is also a function of temperature, and can be computed using Sutherland's law [14]:

$$\mu(T) = \mu_0 \cdot \frac{T_0 + C}{T + C} \cdot \left(\frac{T}{T_0} \right)^{3/2}, \quad (5)$$

C , μ_0 and T_0 are constants and depend on the medium. Table 1 provides all constants for nitrogen and air. The comparison with data from Hilsenrath et al. [15] reveals a maximum deviation of up to 3% at a temperature of 100 K. Therefore, Sutherland's law with the constants listed in the table can be

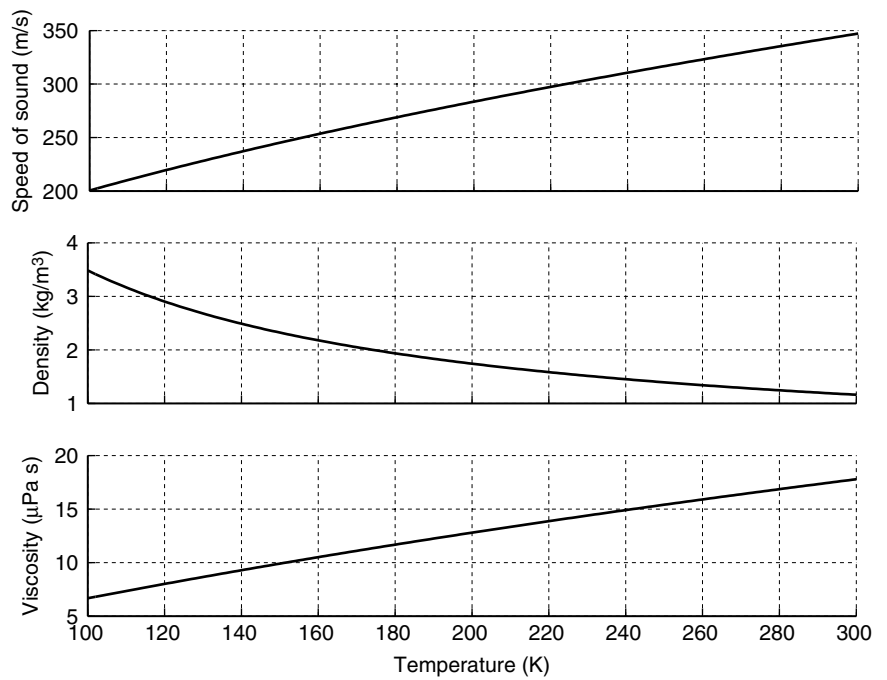


Figure 2: Temperature dependence of the Reynolds number relevant parameters: speed of sound, density and viscosity for nitrogen, according to [13, 14].

Table 1. Constants for Sutherland's formula for air and nitrogen.

Gas	C (K)	T_0 (K)	m_0 (1×10^{-6} Pa · s)
Air	120	291.15	18.27
Nitrogen	111	300.55	17.81

considered to be reasonable for this range of temperatures. The resulting dependence of the viscosity is sketched in Fig. 2, bottom graph.

Additionally, the temperature dependence of the density and the viscosity will increase the Reynolds number with cooling down the fluid. Assuming a constant Mach number, the flow velocity U_∞ will decrease with decreasing temperature, because the speed of sound decreases. Consequently, the latter will reduce the Reynolds number. However this effect is over-compensated by density and viscosity effects.

In cryogenic wind tunnels, it is appropriate to specify the temperature and the Mach number. The Reynolds number versus Mach number for different temperatures is depicted in Fig. 3. The computation is valid for a model scale of 1 : 25, with a

characteristic length of $L = 0.12$ m, based on the width of the train, in a nitrogen atmosphere. By cooling down from room temperature to $T = 100$ K one can increase the Reynolds number by a factor of approximately 5.

2.2. AEROACOUSTIC SCALING

For the investigation of the scaling effects the knowledge of the relations between source properties, like frequency and source strength, and the physical properties of the flow, namely density and speed of sound, is an important issue. The measurements presented in this paper reveal two different aeroacoustic source mechanism. The first source can be described by sound of a cylinder in cross flow, the second source can be characterised by a kind of flow excited cavity noise.

The frequency and amplitude
 volume 11 number 4 *noise notes*

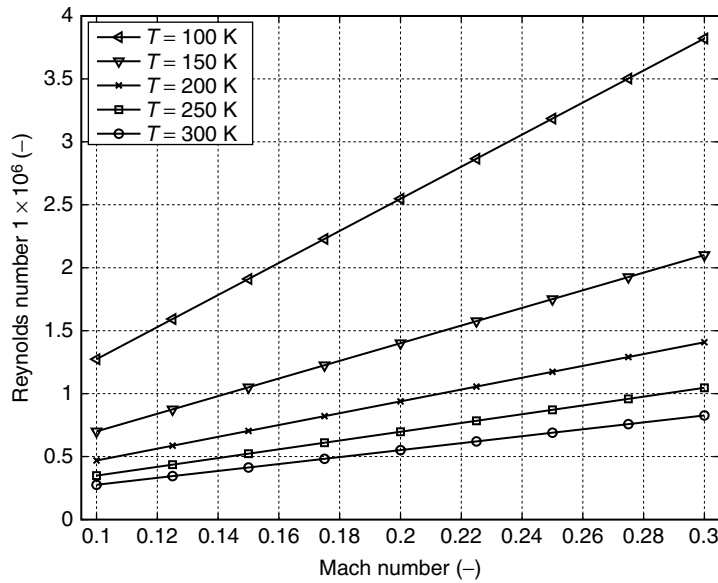


Figure 3: Reynolds number versus the Mach number for different fluid temperatures.

scaling of both source types will be discussed in the following sections.

2.2.1. Flow induced noise of a cylinder in cross flow

Due to its geometrical similarities, the noise emitted by the pantograph might be comparable to the one of a cylinder in cross flow: the pantograph consists of several cylindrical elements with different orientations and diameters. This is illustrated in Fig. 4, by showing a close-up photograph of a simplified pantograph model, which is used for the present study.

The flow induced noise of a circular cylinder in cross flow is a famous example for an aeroacoustic sound source. Since the Reynolds number is higher than $Re > 40$ the wake becomes

unsteady, and a so-called Kármán's vortex street develops. Over a large Reynolds number range $Re < 1 \times 10^7$, eddies are shedding alternating from each side of the cylinder. This leads to pressure fluctuations and consequently, to sound emission sound into the far-field with the frequency of the shedding vortices. This effect was found by Strouhal [16]. The frequencies depend nearly linearly on the flow velocity, and the Strouhal number is a common coefficient to characterise this type of sound sources:

$$Sr = \frac{f \cdot L}{U_\infty}, \quad (6)$$

with the frequency f , the characteristic length L and the flow velocity U_∞ . For a



Figure 4: Close-up photograph of the used pantograph.

wide range of the Reynolds number, the Strouhal number is nearly constant within an interval of $Sr = 2 \pm 10\%$. Later, the Strouhal number is used as dimensionless frequency, analysing frequency spectra of the pantograph. Ahlefeldt et al. [17] carried out aeroacoustic microphone array measurements under cryogenic conditions down to $T = 100$ K for a cylinder in cross flow, for a wide range of the Reynolds number between $4 \times 10^3 < Re < 8 \times 10^4$, based on the diameter of the cylinder. This well known sound source was chosen in order to gain experience using the microphone array technique for this specific application. Ahlefeldt et al. [17] observed good agreement comparing their results with experimental data published in the literature, as well as with prediction of a theoretical model, which discloses the fundamental relations between the properties of the fluid and the observed pressure amplitude. The model is based on Lighthill's acoustic analogy, and is introduced in the following:

Lighthill's acoustic analogy [18] laid the fundamentals of the prediction of aeroacoustic sound generation of a free flow. Curle [19] extended Lighthill's equations to account for solid boundaries. It is assumed that there is a fluctuating lift force which is responsible for the sound generation. This force can be described by a periodic force with frequency f . The amplitude of the force is proportional to the dynamic pressure and a typical length scale L of the source. Curle deduced the following equation, which allows for the prediction of the emitted squared acoustic pressures of a aeroacoustic dipole sound source:

$$p'^2 \propto \rho^2 c^4 M^6. \quad (7)$$

The squared acoustic pressure depends on the 6th power of the Mach number (2), the square of the density ρ

and to the 4th power of the speed of sound c . Phillips [20] adapted Curle's equation for prediction of the intensities of Aeolian tones emitted by a cylinder in cross flow. He found:

$$p'^2 \propto A Sr^2 \rho^2 C^4 M^6. \quad (8)$$

This result is similar to Curle's result Eq. (7), but here the emitted sound pressure depends additionally on the square of the Strouhal number (Eq. (6)). The variable A is introduced as a factor, which combines Reynolds number dependent effects, namely the influence of different correlation length along the cylinder and the dependence of the flow conditions on the lift force. The correlation length will decrease with increasing Reynolds number, because three-dimensional instabilities will rise (especially when the wake of the cylinder becomes turbulent) and phase deviations along the cylinder will increase.

2.2.2. Noise induced by flow over a cavity - modelling the noise from the bogie section

The outcome of the experiments presented below is, that the frequencies of the tonal contributions emitted by the bogie section of the train are not influenced by the flow velocity. The wavelength λ seems to be connected to a typical length or volume. This behaviour can be described by a certain type of aeroacoustic cavity excitation.

In the following some aspects about aeroacoustic noise of cavities published in literature are mentioned. Tam et al. [21] reviewed publications about different mechanisms, some of which are pointed out in the following:

The so-called captive vortex model describes cavity excitation by captured vortices inside the cavity, which has been observed for different length to depth ratio L/D of the cavity. Especially cavities of square section have a strong tendency to form a single, stable vortex

(see Roshko [22]). The oscillatory motion of this captured vortex system has been considered as a cause of large scale pressure fluctuations inside the cavity. If L/D is less than 2, the dimension of the cavity does not permit cellular flow and the internal pressures become random.

Rossiter [23] suggested that cavity noise is a result of acoustic feedback. At the upstream lip of the cavity vortices shed periodically, and an unsteady shear layer develops. The vortices in the shear layer propagate downstream with the convection velocity $U_c < U_\infty$ and impinge on the downstream edge. As a result, an acoustic pulse is generated which travels upstream inside the cavity until it reaches the upstream lip. There it triggers the separation of new vortices and the feedback loop is closed herewith. Rossiter [23] conducted measurements for the Mach numbers range $0.4 < M < 1.2$, and found a nearly linear frequency - flow velocity dependence. Based on his experimental results, he developed a semi-empirical formula for the evaluation of cavity modes:

$$Sr = \frac{fL}{U_\infty} = \frac{m - \gamma}{\frac{1}{K} + M}, \quad (9)$$

where γ depends on the length to depth ratio ($0.25 < \gamma < 0.58$ for $4 < L/D < 10$). K is a constant and corresponds to the ratio $K = U_c/U_\infty$, and is around $K = 0.57$. Furthermore, he found the excitation of tonal components is stronger for deeper cavities with a length to depth ratio of $L/D < 4$ and random components predominate in longer cavities with $L/D > 4$. Rossiter proposed that resonance can occur, if the frequency of one of these modes is close to the natural frequency of the volume of air in a cavity.

Plumlee et al. [24] conducted analytical calculation of cavity resonances. They suggested that the turbulent shear layer, which spans over

the cavity, provides a broadband source which drives the cavity oscillations. Certain frequencies can be amplified by the cavity, and length, width and depth modes can be excited.

The characteristic frequency equation for a closed cuboid with the dimensions L_i (for the x_i -direction) with six acoustically hard walls ("closed cavity") is simply given by:

$$f^2 = \frac{c^2}{4} \left[\left(\frac{n_x}{L_x} \right)^2 + \left(\frac{n_y}{L_y} \right)^2 + \left(\frac{n_z}{L_z} \right)^2 \right], \quad (10)$$

where n_i denotes the mode in the i -th direction. Plumlee et al. [24] postulated, that for the calculation of the depth modes, an expression for the acoustic impedance of the open face is necessary. The cavity can be seen as an acoustic enclosure with five acoustic hard walls (wall impedance is infinity) and one wall with finite wall impedance. For the pressure response of the depth mode, regarding the finite impedance of the open face of the cavity, they found:

$$\frac{p}{p_0} = \left[\left(R(M, f, L/D) \sin \frac{\gamma L_z}{L_x} \right) + \left(X(M, f, L/D) \sin \frac{\gamma L_z}{L_x} - \cos \frac{\gamma L_z}{L_x} \right)^2 \right]^{-1/2} \quad (11)$$

where $\gamma = kL_x$ denotes the normalised frequency of the wave number $k = 2\pi f/c$. R describes the radiation resistance and X the radiation reactance, the real and the imaginary part of the radiation impedance. Both parameters are functions of the Mach number of the flow over the cavity (even though there is only a weak dependence for subsonic flows), of the frequency and of the length to depth ratio L/D of the cavity. Hence, the frequency as well as the amplitude of the excitation depth mode is a function of the Mach number. This mode predominates for cavities with a length to depth ratio smaller than one. East [25] came to a similar result. His

experimental investigations on rectangular cavities revealed, that the main cavity-pressure resonances occur in the lowest depth mode for deeper cavities $L/D < 1$, especially at Mach numbers lower than 0.18. For cavities with $L/D > 1$, Plumblee et al. [24] proposed that the length mode is the dominant sound generation mechanism. For this situation they found:

$$f^2 = \frac{c^4}{4} \left[\left(\frac{n_x}{L_x} \right)^2 - \left(\frac{g_n}{L_z} \right)^2 \right]. \quad (12)$$

Based on experimental experiences the transversal modes are not excited, and the term

$$\left(\frac{n_y}{L_y} \right)^2 \quad (13)$$

can be neglected here. The variable g_n is again a function of the frequency, of the radiation resistance R and of the radiation reactance X . A procedure to iteratively calculate g_n is described in the paper by Plumblee et al. [24]. Exemplarily, simulations of the

amplification factor of the depth - mode of a cavity with $L_x = L_z = 0.1$ m, using Eq. (11) have been performed. The results for $M = 0.1, 0.2$ and 0.3 are depicted in Fig. 5. For the depth mode as well for the length mode (the latter is not shown here), it turns out, that there is only a weak Mach number dependence on the amplitude and frequency response, especially for the Mach number range between $0.05 < M < 0.30$ discussed in this paper.

At first sight, the model proposed by Plumblee et al. [24] is a good description of the sound generation by flow over cavities, while there is no strong correlation between observed frequencies and (a subsonic) flow velocity. Plumblee's prediction also showed a good agreement with his experimental data. Nevertheless, it should be noted that this model fails, as far as a laminar flow is concerned. According to Plumblee et al. [24], the unsteady flow over the cavity induces resonance, and consequently, a laminar flow was not able to induce this excitation. Block et al. [26] found experimentally, that the cavity excitation is even decreased, when a turbulence-generating roughness

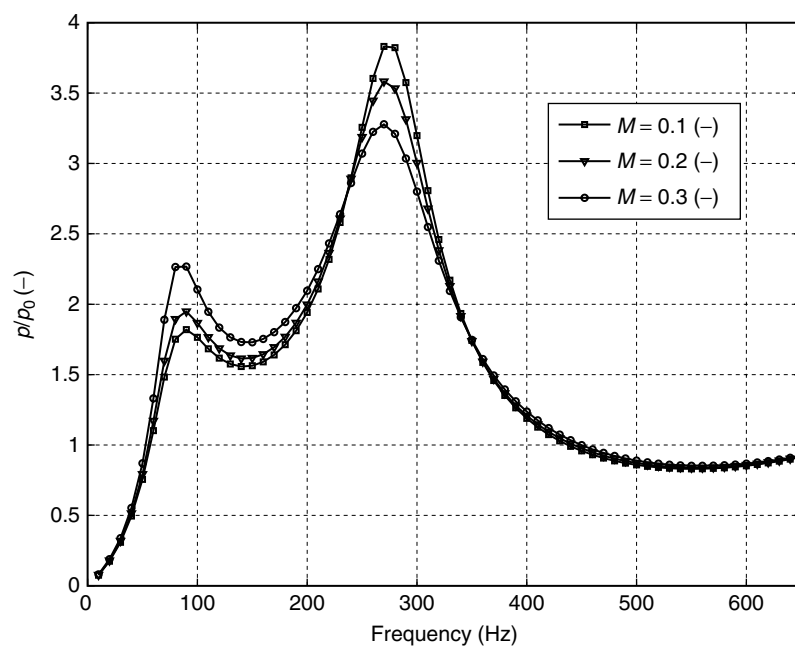


Figure 5: Simulated amplification factor of the depth - mode of a cavity with $L_x = L_z = 0.1$ m.

element is installed upstream of the cavity.

Following the above literature overview is the interpretation of the observed frequencies using a appropriate dimensionless quantity can be addressed. The experiments described below disclose a sound source at the bogies, which emits tones, whose frequencies are velocity independent. Spectra obtained from measurements at different temperatures in the cryogenic wind tunnel will be compared with each other. The frequency is a function of the temperature at constant wavelength, because the speed of sound c is temperature dependent (see Eq. (3)):

$$f(T) = \frac{c(T)}{\lambda}. \quad (14)$$

When comparing data acquired at different temperatures this effect must be considered. In this particular case, it is reasonable to use a dimensionless frequency which is nondimensionalised with the speed of sound and a characteristic length, leads to the Helmholtz number¹:

$$He = \frac{f \cdot L}{c} \quad (15)$$

This formulation is similar to the Strouhal number, see Eq. (6), except that here the speed of sound is the crucial parameter.

It must be noted that results obtained in the cryogenic wind tunnel are discussed in terms of the Helmholtz number.

3. METHODS

The following sections describe the experimental setup in the aeroacoustic and in the cryogenic wind tunnel, the applied measurement technique and the used beamforming algorithms.

3.1. EXPERIMENTAL SETUP AND TEST FACILITIES

For all experiments described in this paper the 1 : 25 scale-model of the Inter City Express 3 (ICE 3)² is used. Optionally, a pantograph can be installed on the head car, or on the first passenger car. For aerodynamic studies, the shape of the model is more important than every detail. Therefore, generic model does not reflect every single feature of a real train. However, for aeroacoustics any single component like antennas, cooling intakes or equipment on the roof, are important sound sources. Nevertheless, the model reflects the most important details, namely the bogies, the pantograph (only available for the measurements in the aeroacoustic wind tunnel) and the gap between the head car and the first car. For all considerations described below concerning the Reynolds number, as characteristic length the width $L = 0.12$ m of the train has been chosen.

The aeroacoustic investigations with this model have been conducted in two different wind tunnels. At first, the main aeroacoustic sources are identified in measurements carried out in the Aeroacoustic Wind Tunnel facility (AWB) of the German Aerospace Center (DLR) in Brunswick allowing for detailed aeroacoustic investigations for Reynolds numbers of up to 0.46×10^6 . Compared with a full-scale train, which operates at $Re > 16 \times 10^6$, this is by a factor of 30 lower and the validity of aeroacoustic measurements in wind tunnels with respect to those on full-scale trains is still unknown. To gain more information of the Reynolds number effect on the aeroacoustics of trains, additional measurements at higher Reynolds numbers up to $Re = 3.7 \times 10^6$ have been carried out in the cryogenic wind tunnel. Both setups in the facilities will be introduced in the following two sections.

¹In literature one also can find an alternative formulation of the Helmholtz number with the factor 2π .

²Details about this benchmark wind tunnel model can be found in DIN EN 14067-6:2010.

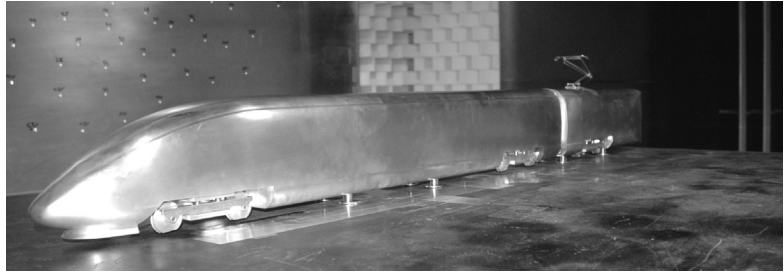


Figure 6: *The 1 : 25 scale-model of the ICE 3 reflecting the bogies, the gap between the head car and the first coach and the pantograph.*

3.1.1. Aeroacoustic wind tunnel

The Aeroacoustic Wind Tunnel facility (AWB) of the German Aerospace Center (DLR) in Brunswick [27] is a closed circuit Goettingen type wind tunnel with an open test section, which is optimised for aeroacoustic experiments: The whole air duct is lined with noise absorbing foam and the test section is surrounded by an anechoic chamber. The wind tunnel provides a low background noise level and the test section nearly free-field conditions.

The nozzle diameter is 1.2×0.8 m, and the maximum wind speed is $U_\infty = 65$ m/s. Fig. 7(b) depicts the facility, and Fig. 7(a) shows the setup in the test section. The train model is installed on a splitter plate, which has an elliptical leading edge and a sharpened trailing edge. This plate is positioned 10 cm above the lower edge of the nozzle in order to peel off the wind tunnel's shear layer. On the leading edge of the splitter plate, a new boundary layer is formed, which is thinner than the wind tunnel boundary layer. The aim is to keep the

thickness of the boundary layer low in order to ensure a reasonable simulation of the flow underneath the train. In the wind tunnel experiment on both surfaces boundary layers develop, which finally result in a more or less elliptical velocity profile, a Poiseuille-like flow. In contrast to this, a real train moves relative to the ground and penetrates the fluid, which is at rest forming a turbulent Couette-like flow (please refer to Jönsson et al. [28]) below the train. A moving belt or a mirror model would provide a better simulation of the full-scale underbody flow in the wind tunnel. However, Grunwald et al. [29] found in force measurements of bluffbodies in ground proximity, that different setups, i.e. a moving belt, fixed ground and a double-model, reasonably reproduce the overall aerodynamic forces, and even more, that the results differ only within the measurement accuracy. Their good agreement can be explained by a convenient relation between the boundary layer thickness on the ground

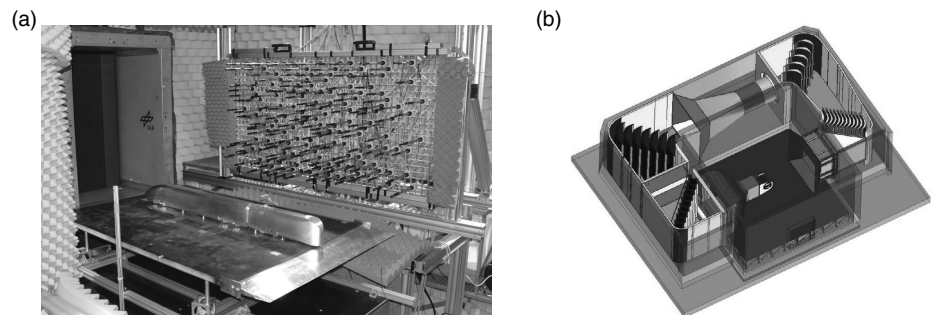


Figure 7: *(a): Setup in the AWB: Inside the test section on a splitter plate the model of the ICE 3 is installed. In the background outside the flow the microphone array is mounted. (b): Drawing of the AWB. The test section is highlighted by the dark gray region.*

and the clearance height of the train. According to Katz [30] one can expect a realistic underfloor flow in a wind tunnel experiment, as long as this condition is fulfilled. A rough estimate (see Schlichting and Gersten [31]), discloses a boundary layer thickness on the ground at the first bogie, which is thin with respect to the clearance height of the train. Therefore, the setup seems to be suitable to investigate the aerodynamics and aeroacoustics of the train's head.

3.1.2. Cryogenic wind tunnel

The Cryogenic wind tunnel DNW-KKK in Cologne is a Goettingen - type wind tunnel with closed test section with dimensions of 2.4×2.4 m. By injecting liquid nitrogen the fluid can be cooled to $T = 100$ K. Thus, the Mach number can be varied between $0.10 < M < 0.30$. A sketch of the facility and a photo of the setup inside the test section is shown in Fig. 8. For the same reason as in the AWB, the model is again mounted on a plate, which is called ground board for setups in closed test sections. The microphone array, consisting of 144 microphones arranged in logarithmic spiral arms, is mounted on the side wall of the wind tunnel. The flow correction for closed test sections, as well as the noise reduction method Biclean (both mentioned in Sec. 3.2) need to be applied in order to obtain reasonable results.

3.2. USED BEAMFORMING ALGORITHMS

For the sound localisation and quantification in aeroacoustic experiments the Delay and Sum Beamforming algorithm (DSB) together with a microphone array are widely used. The principle is based on the summation of retarded microphone signals. For the frequency domain, the algorithm can be written as follows:

$$A_k = \frac{e_k^\dagger \mathbf{W}_k \mathbf{R} \mathbf{W}_k^\dagger \mathbf{e}_k}{M^2} \quad (16)$$

Thereby, A_k denotes the beamformer output of the k^{th} focus point, \mathbf{R} the cross-spectral matrix, M the number of microphones and \mathbf{e}_k the steering vector. The weighting matrix \mathbf{W}_k compensates the $\frac{1}{d}$ decay of the amplitudes (assuming monopole character of the source), with d the distance between the k^{th} focus point and each microphone position. Additionally, corrections of the amplitudes can be made with a modified weighting matrix $(\cdot)^\dagger$ which indicates the complex conjugate and transposed vector or matrix. For more details see the textbook from Johnson and Dudgeon [32].

Especially in a noisy surrounding a higher signal-to-noise ratio is obtained by subtracting the diagonal elements (Mueller [33]), i.e. the auto spectra, of the cross-spectral matrix. This technique has been applied to all data presented in this paper.

In order to improve the spatial resolution of the beamforming algorithm especially at lower frequencies and to obtain more quantitative results, the CLEAN-SC algorithm introduced by Sijtsma [34] is used for the present study. Reflections as well as side lobes of the point spread function, which can appear as ghost sources, are subtracted.

Further, measurements in closed test sections may be disturbed by reflections, strong background noise and mode excitation. The BiClean algorithm, introduced by Ehrenfried and Koop [35, 36] detects plane waves in the array data, which may belong to wind tunnel modes or originated far away from the test section. This contribution is filtered out, thereby improving the signal-to-noise ratio.

Besides other data, the Delay and sum Beamforming algorithm requires the accurate positions of the array microphones. The microphone array, which is used for out of flow applications (see Fig. 7(a)), is a lattice construction. The latter avoids strong

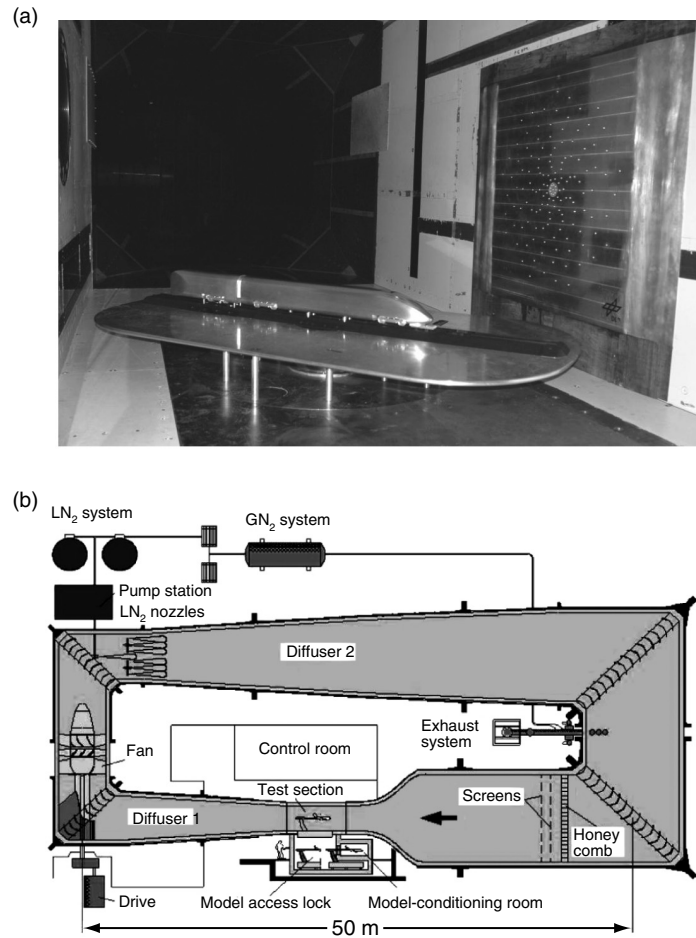


Figure 8: (a): Setup in the test section of the DNW-KKK. The train model is mounted on a ground board. The microphone array is arranged behind, mounted on the wind tunnel wall. (b): Drawing of the DNW-KKK, from www.dnw.aero.

interaction with the sound field. The accurate positions of the microphones are not given by the setup itself. Therefore, to achieve the required accuracy, it is necessary to measure the exact positions. For this, a calibration procedure has been developed, which works similarly to the well known global positioning system (GPS): With several acoustic “satellites” and a reference microphone, the array microphones are located with an accuracy better than 1 mm. For more details see Lauterbach et al. [37].

In the KKK, the microphone array is mounted on a side panel inside the wind tunnel boundary layer. From the origin of the sound in the centre of the test section to the microphones, the sound is convected by the flow. A

uniform flow is assumed for the estimation of the modified travel times in the flow. This correction is applied to the steering vector. For more details see Koop [38]. The aeroacoustic wind tunnel has an open test section, and the array is positioned outside the flow. The sound which is emitted by the model has to propagate through the wind tunnel shear layer. Phase shifts and variations in amplitude, induced by refraction on the shear layer and convection of the sound wave by the flow, are corrected according to Amiet [39] by modifying the steering vector, and the weighting matrix, respectively.

Aside from noise maps, which map the distribution of sound sources, a modified integration technique, which described in Brooks et al. [40], enables

the computation of sound power level spectra for specified scan areas. A normalisation with the point spread function, which was also proposed by Brooks et al. [40] is not applied here, because all coherent contributions in the source maps have been subtracted already with the CLEAN-SC algorithm.

4. RESULTS AND DISCUSSION

4.1. MEASUREMENTS IN THE AEROACOUSTIC WIND TUNNEL (AWB)

Fig. 9 shows source maps for one third-octave bands between 3.15 kHz and 10 kHz, measured at a Mach number of $M = 0.175$, corresponding to a flow velocity of $U_\infty = 60$ m/s. The sound power level is visualised colour-coded over a dynamic range of 24 dB. The train was equipped with the pantograph on the first car. Obviously, in the analysed frequency bands different source mechanisms are active. For lower frequencies, the first bogie is the main aeroacoustic source, but for frequencies higher than 5 kHz the pantograph becomes dominant. Also, the gaps between head car and first coach and the other bogies appear in the source maps. It is found, that the first bogie is a much stronger source, than the other bogies. This behaviour

was also observed in full-scale drive-by tests with a Train à grande vitesse (TGV) (a French high-speed train), by Mellet et al. [2]. Also, Martens et al. [6], who report on measurements conducted with an ICE 3, observed similar tendencies in their source maps. An explanatory approach is based on the characteristics of the boundary layer: at the head of the train close to the stagnation point, the boundary layer is laminar and thin. Ahuja et al. [41] investigated among other things the effect of the upstream boundary layer thickness on cavity noise in wind tunnel experiments on a rectangular cavity. The incoming boundary layer was turbulent, and the thickness was modified by placing a backward facing step upstream of the leading edge of the cavity, such that quotient of boundary layer thickness δ and cavity length L could be varied between $0.038 < \delta/L < 0.066$. It turned out, that a thicker boundary layer can decrease broadband as well as tonal noise. By considering Block et al.'s [26] observations, i.e. that the aeroacoustic cavity excitation is increased for a laminar flow, we conclude that the thin and probably laminar boundary layer at the first bogie is the physical explanation for the strong sound generation.

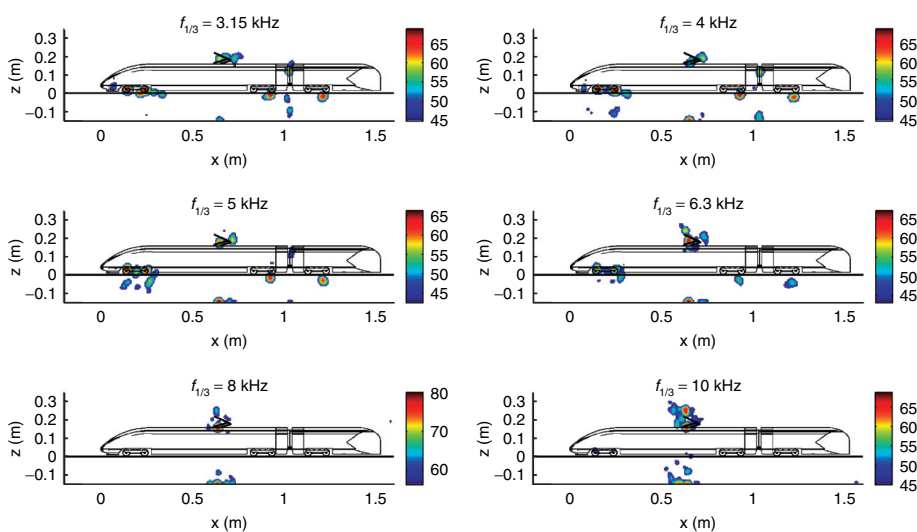


Figure 9: One-third octave source maps of the ICE 3, measured in the AWB at $U_\infty = 60$ m/s. Sound power level is given colour-coded over a dynamic range over 24 dB; with reference power $P_0 = 1 \times 10^{-12}$ W.

The three graphs in Fig. 10 show integrated beamforming spectra, which belong to the areas of the whole train (blue), the pantograph (green) and the first bogie (red). For frequencies higher than 5 kHz the pantograph emerges the strongest source, emitting strong tonal components. The spectrum of the first bogie also contains tones in the low-frequency range of < 4 kHz, but its overall shape is smoother and the sound power level declines stronger for higher frequencies, comparable to typical turbulence spectra.

In order to investigate the characteristics of the sound generation

of the first bogie and the pantograph, spectra for different flow velocities between $20 < U_\infty < 60$ m/s, corresponding to Reynolds numbers between $0.153 \times 10^6 < Re < 0.456 \times 10^6$ and Mach numbers between $0.058 < M < 0.175$, are presented in the following.

4.1.1. Aeroacoustics of the first bogie

We start the discussion with spectra of the first bogie, given in Fig. 11(a). The overall shape of the spectra does not change significantly with increasing flow velocities and the locations of the two humps in $f = 2417$ Hz and $f = 3406$

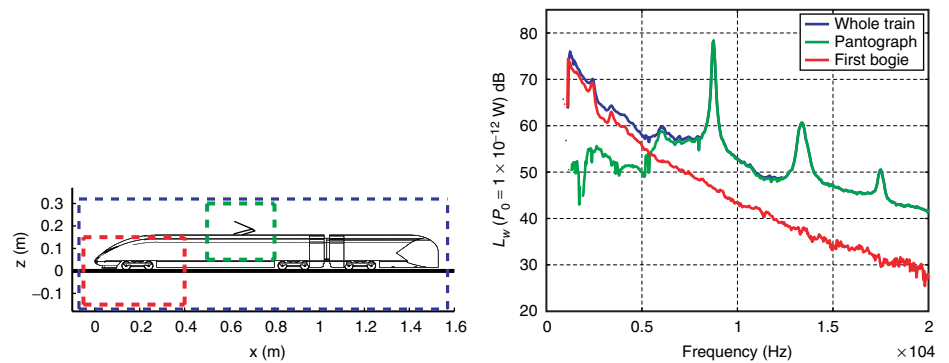


Figure 10: Integrated narrowband spectra (bandwidth $\Delta f = 36.6$ Hz) for three different scan areas: the whole ICE 3 train (blue), the pantograph (green) and the first bogie (red). The flow velocity is $U_\infty = 60$ m/s, which corresponds to a Mach number of $M = 0.175$ and a Reynolds number of $Re = 0.459 \times 10^6$.

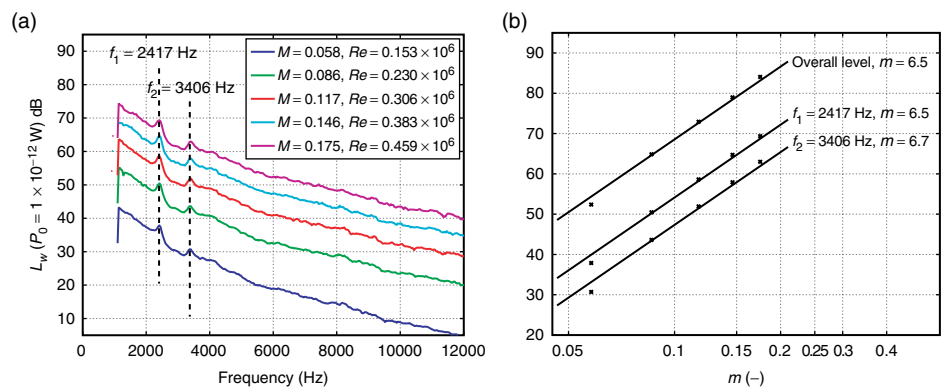


Figure 11: Characterisation of the noise of the first bogie for different Mach numbers, measured in the AWB. (a): Narrowband spectra ($\Delta_f = 36.6$ Hz) for different Mach numbers, computed using the source integration method. The dashed lines highlight the weak tonal contributions in the spectra, which are not velocity dependent. (b): Relation between Mach number and sound power level. Depicted for the two sound power peak levels in $f_1 = 2417$ Hz and in $f_2 = 3406$ Hz and for the overall sound power level.

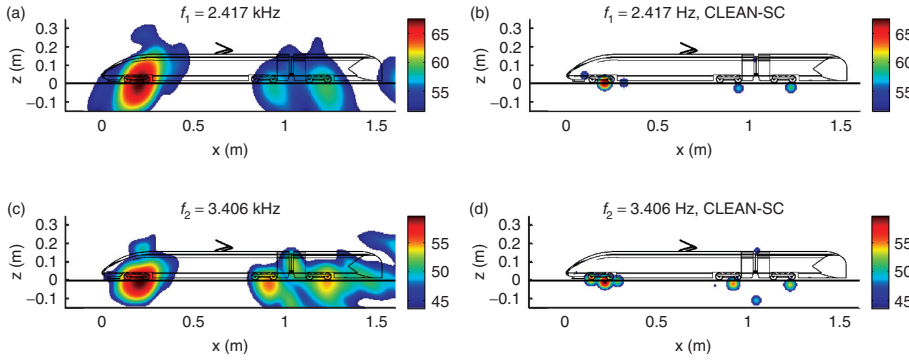


Figure 12: Narrowband ($\Delta_f = 36.6$ Hz) sound power source maps of the ICE 3, given over 14 dB dynamic range. (a) and (b): Maps for $f = 2417$ Hz, using the standard DSB and CLEAN-SC. (c) and (d): The same, but for $f = 3406$ Hz.

Hz, marked by the dashed lines, are not affected by the flow velocity. To make sure, that these characteristic humps in the spectra are no artefacts, like sidelobes of strong sources located in the proximity of the integration box, narrowband maps with a bandwidth of $\Delta_f = 36.6$ Hz for the two characteristic frequencies are presented in Fig. 12. The sound powers are computed over 14 dB dynamic range. This analysis discloses the bogie section as the strongest source for both frequencies, independent of the used beamforming algorithm. Therefore, it is most probable that the humps observed in the spectra in Fig. 11(a) belong to that section.

The fact, that the frequencies of the observed tonal components in the spectra emitted by the first bogie are not scaling with the wind speed, leads to the hypothesis that this sound source is a kind of cavity mode excitation. Therefore, a mechanism reflected in Rossiter's model [23], introduced in Sec. 2.2.2, cannot lead to our observations, because here the amplified frequencies show a linear dependence on the flow velocity. It agrees more with Plumblee's explanations [24], where the frequencies scale mainly with the cavity dimensions. In the following Plumblee's basic principles are simplified for a one-dimensional cavity with infinite wall impedances. For this rough estimate, also the influence of the bogie inside the cavity is neglected. To find a

characteristic length which may be responsible for the observed frequencies, we analysed the development of standing wave. A standing wave occurs, if a multiple of $n = 1, 2, 3, ..$ of the half wavelength λ is equal to the dimension L of the one-dimensional oscillator. One will observe the following frequencies:

$$f = \frac{c}{2} \frac{n}{L'} \quad (17)$$

with $\lambda = \frac{c}{f}$. This expression corresponds to the equation proposed by Plumblee (Eq. (10)) in one dimension with infinite wall impedances. Assessing a typical length scale of the cavity for a known frequency, the equation is rearranged as follows:

$$L = \frac{nc}{2f} \quad (18)$$

For the first three modes $n = 1, 2, 3$ corresponding to the two experimental observed frequencies one obtains the following dimensions L :

$$\text{for } f = 2417 \text{ Hz} \begin{cases} n = 1: & L = 0.070 \text{ m} \\ n = 2: & L = 0.140 \text{ m} \\ n = 3: & L = 0.210 \text{ m} \end{cases} \quad (19)$$

$$\text{for } f = 3406 \text{ Hz} \begin{cases} n = 1: & L = 0.050 \text{ m} \\ n = 2: & L = 0.100 \text{ m} \\ n = 3: & L = 0.150 \text{ m} \end{cases} \quad (20)$$

For the first three modes all of these lengths are in the order of centimetres, which is of the same order of magnitude of the dimensions of the bogie section. The distance between the bottom of the bogie cavity and the ground amounts to 0.046 m, the length of the cavity to 0.153 m (bottom of the cavity), and the width to 0.108 m (leading edge of the cavity) and 0.114 m (rear section), respectively.

At this point, it is not possible to find an unambiguously relation between the frequencies and the length scale of the train. However this rough estimate already reveals, that the bogie section does not act like an aeroacoustic excited cavity. The frequencies are related to the dimensions of the cavity, and different modes can be excited.

Further the question arose, if this behaviour persists for higher Mach- and Reynolds numbers, and if additional measurements for other flow parameters are necessary. Such experiments, conducted in the cryogenic wind tunnel, are presented in Sec. 4.2.

This section focuses on the influence of the Mach number on the emitted sound levels. In this context, it is desirable to estimate the powerlaw exponent m , which describes the relation between the sound power and the Mach number:

$$p'^2 \propto M^m. \quad (21)$$

Therefore, the sound power levels are plotted over the logarithmic Mach number abscissa, and the data are processed as follows:

$$L_w \propto m \log M. \quad (22)$$

The slope of the regression line is proportional to the powerlaw exponent m . For the narrowband analysis the peak sound power level of the frequencies f_1 and f_2 were taken, and for the overall analysis an integration over the complete available frequency range between $1100 < f < 16000$ Hz was conducted. Fig. 11(b) depicts the

relation between the sound power levels versus the Mach numbers in logarithmic scale. For the overall levels as well as for the peak levels in $f_1 = 2417$ Hz the exponent is around $m = 6.5$, and $m = 6.7$ for the peak levels in $f_2 = 3406$ Hz. Since for an acoustical dipole source one would expect $m = 6$ (see Eq. (8)), the results presented here are in a good agreement.

4.1.2. Aeroacoustics of the pantograph

Fig. 13(a) depicts spectra of the pantograph for the same Mach number range, analogouse to the investigations of the bogie noise. This kind of sound source differs from the sound emitted by the bogie, and a strong Mach number dependence is observed. Not only the overall levels increase, but also the shape of the spectra change. In order to find out if an Aeolian tone characteristic with linear Mach number dependence exists, the spectra are plotted over the Strouhal number (Eq. (6)), as depicted in Fig. 13(b). The pantograph consists of several cylindrical elements of different diameters between 0.1 and 4 mm and different orientations to the flow. Therefore, it seems conceivable that the pantograph shows a similar behaviour like a cylinder in cross flow. In contrast to a cylinder though, it is hard to determine a distinct characteristic length scale for a complex geometry like a pantograph. Therefore, a mean diameter $L = 2$ mm is chosen *a priori*. The spectra in Fig. 13(b) reveal strong peaks located around $Sr = 0.30$, 0.43 , 0.59 and 0.87 for all Mach numbers. The shape of the spectrum for the lowest Mach number $M = 0.058$ differs from all the others. For instance, the peak around $Sr = 0.43$, clearly visible for higher Mach numbers, does not appear for the lowest Mach number. It seems, that the aeroacoustic mechanism of the pantograph requires a minimum Mach number to work properly.

A closer look reveals possible

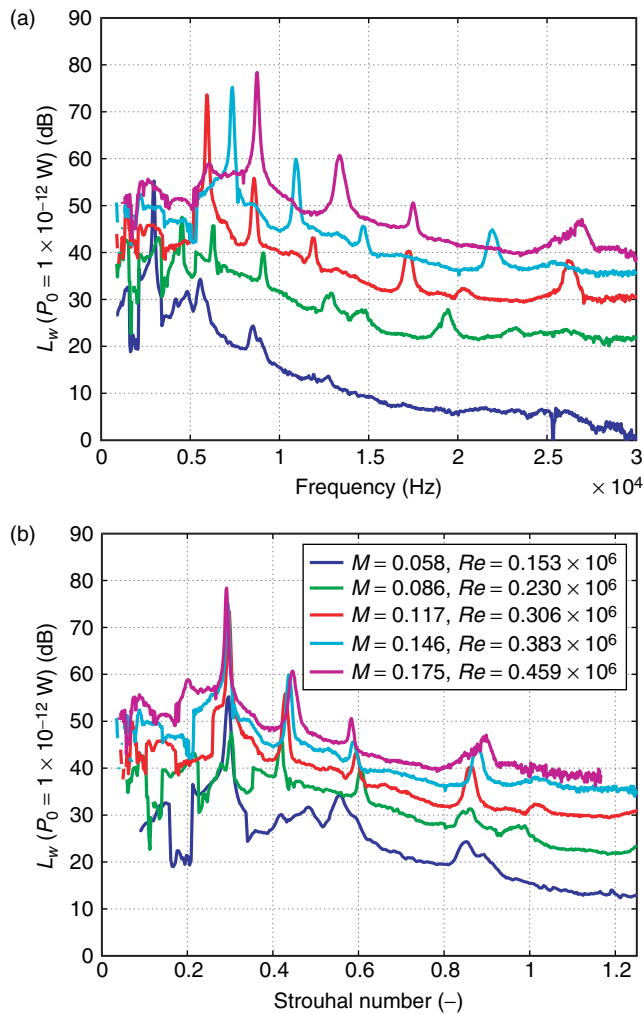


Figure 13: Characterisation of the noise of the pantograph for different Mach numbers, measured in the AWB. (a): Spectra of the pantograph, computed using the source integration method. (b): Again the pantograph spectra, plotted over the Strouhal number, with $L = 2$ mm.

higher harmonics of a fundamental Strouhal number. The peaks in $Sr = 0.59$ seem to be higher harmonics of the peaks in $Sr = 0.30$ (in the following, the associated source is called “source 1”); the same with the peaks in $Sr = 0.87$, which belong to the peaks in $Sr = 0.43$ (“source 2”). In order to identify which frequency peak belongs to which part of the pantograph, as a first step narrow band source maps for the regarded Strouhal numbers are presented in Fig. 14. This measurement has been conducted at a Mach number of $M = 0.175$. For the Strouhal numbers $Sr = 0.30$ and $Sr = 0.59$ the sources seem to be located in the foot region of the pantograph, whereas for the Strouhal

numbers $Sr = 0.43$ and $Sr = 0.87$ the sources appear at the top end of the pantograph, where the slider is located. As a cross-check, maps are given in Fig. 15, showing the source distribution in the YZ-plane, viewed from the rear to the train. The array microphones are placed on the right hand side. The plane is located in $x = 0.635$ m, which is the x -position where both sources were found before. In order to exclude artifacts of the deconvolution algorithm, standard DSB maps are shown as well. The spatial resolution of the microphone array in y -direction is poor compared with those in the x - and z -directions, and therefore, the sources appear to be wider in. The maps reveal a similar

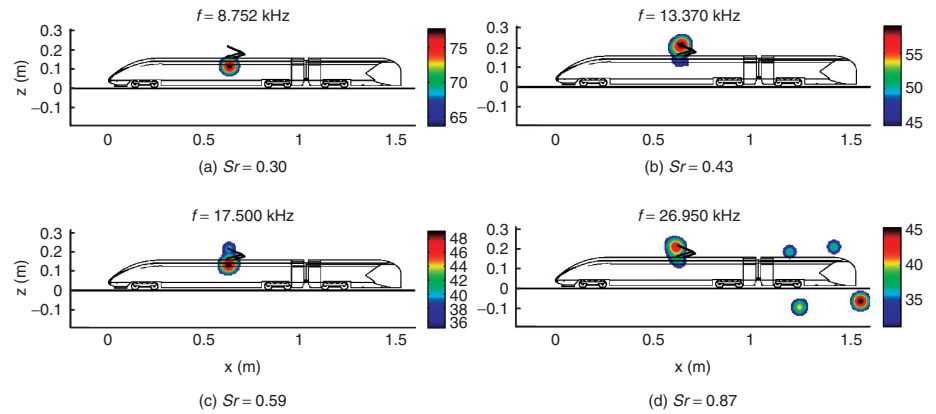


Figure 14: The Fig. (a)-(d) depict narrowband source maps for different Strouhal numbers, measured at $M = 0.175$ in the AWB, sound power levels are colour-coded, computed over 14 dB dynamic range.

behaviour for the Strouhal numbers $Sr = 0.30$ and $Sr = 0.59$ (source 1) and for the Strouhal numbers $Sr = 0.43$ and $Sr = 0.87$ (source 2), respectively. Both tonal components of source 2 can be attributed to the slider, which also agrees with the source position in Fig. 14. Source 1, however, appears in the YZ-plane underneath the contour of the train body. Obviously, the beamforming technique is not able to determine the physical correct source location. As pointed out before, the source mechanism of the pantograph is comparable to the dipole source of a cylinder in cross flow. The lobes in the directional pattern are oriented perpendicular to the cylinder and to the flow direction. Depending on the orientation of a dipole source to the microphone array the beamforming algorithms can fail with the estimation of the source location and strength, because the monopole assumption in the beamforming algorithm (see section 3.2) is violated. As far as the orientation of the dipole is *a priori* known, a modified beamforming algorithm can improve the results, as proposed by Liu et al. [42]. Furthermore, the surface of the train acts as a reflecting boundary. Depending on the orientation of the dipole to the surface, the source and its mirror source superimpose, which results in a complex directional pattern in the far field. All these facts can lead to a misinterpretation of the source maps

depicted in Fig. 14.

It can be assumed, that the aforesaid combination of a certain directivity of source 1 and the reflecting boundaries lead to distortions in the beam-forming maps. Therefore, the source position of source 1 is still unknown. To solve this problem, single-microphone spectra of measurements for two different configurations of the pantograph are compared with each other, in Fig. 16. One configuration is the baseline configuration of the pantograph; for the second configuration the elements of the slider were covered with aluminium tape. The microphone was laterally mounted in $(x; y; z) = (0.72 \text{ m}; -0.73 \text{ m}; 0.43 \text{ m})$. If source 1 is located at the foot region of the pantograph, this modification should have no effect on the regarded frequency peaks. If there is an effect, then the sliders must be also origin of source 1. The black spectrum represents the sound of the base line configuration of the pantograph on the train model, and the red spectrum the configuration with the taped slider elements. The comparison of the spectra reveals a significant influence of the modification on the peaks in $Sr = 0.30$ and $Sr = 0.59$, and therefore, source 1 must have its origin at the sliders. The blue spectrum was recorded during a measurement without mounted pantograph on the train model. The background noise level is below the others, and for the present case, the

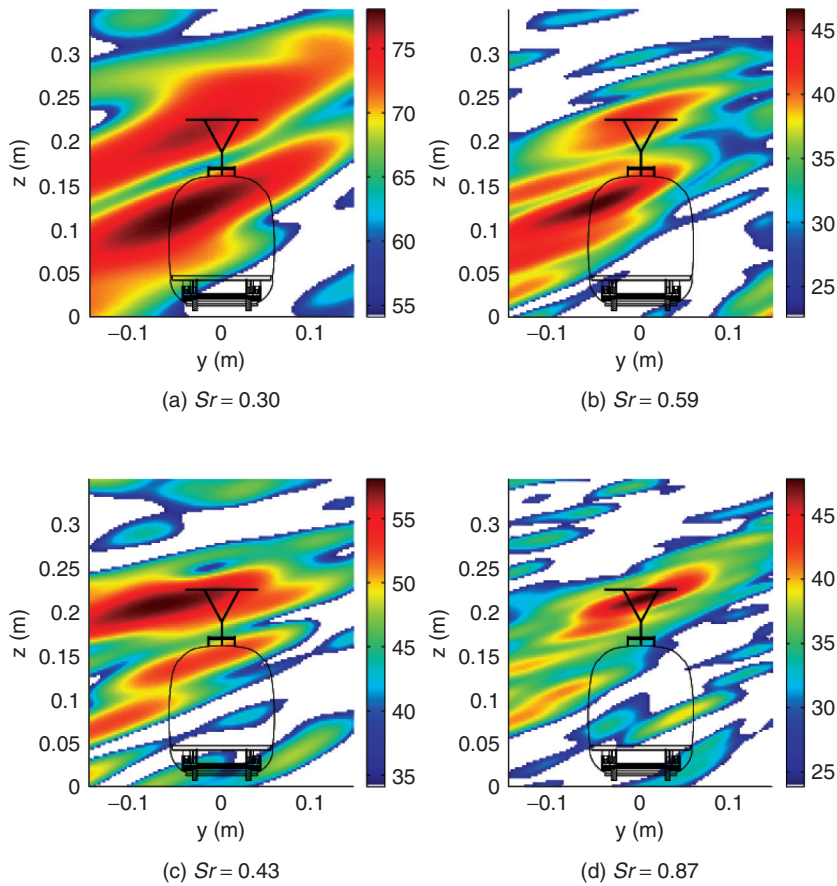


Figure 15: Narrowband DSB source maps for the four discussed Strouhal numbers, in the YZ-plane.

investigation of pantograph noise in wind tunnel optimised for aeroacoustics, using a single microphone is feasible.

All measured tonal components belong to the top end of the pantograph. The beamforming technique is not able to

verify which single element of the sliders creates which tones. To shed more light on this the frequencies of the observed peaks are analysed. Previously, the Strouhal number has been used with a specified characteristic length of $L = 2 \text{ mm}$

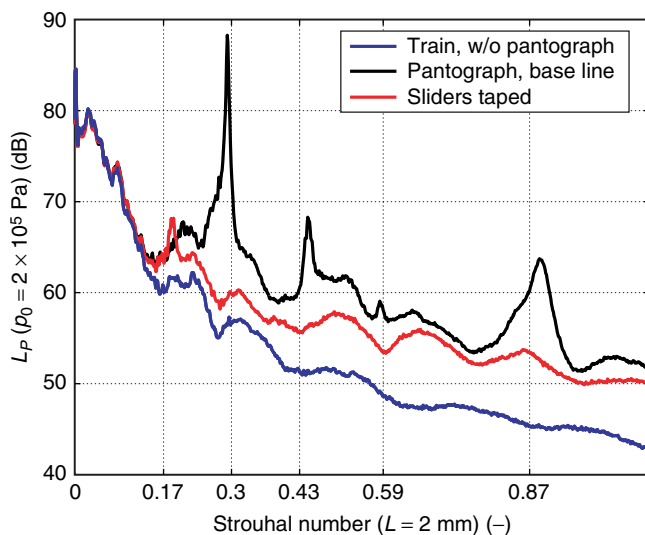


Figure 16: Single-microphone spectra, measured for different configurations.

$$Sr = \frac{f \cdot 2 \text{ mm}}{U_\infty} \quad (23)$$

The following investigations describe an alternative approach. As a rough approximation it can be assumed, that the elements of the pantograph behave like an Aeolian sound source. Therefore, according to Strouhal [16] the number reads

$$Sr_L = \frac{f \cdot L}{U_\infty} = 0.20 \quad (24)$$

The index \cdot_L indicates, that the length L is the characteristic variable. Using Eq. (23) and (24) one obtains for the length scale:

$$L = \frac{Sr_L}{Sr} \cdot 2 \text{ mm} \quad (25)$$

For the fundamental modes of the two sources the length scales follow:

$$\text{Source 1: } Sr = 0.30 : \quad (26)$$

$$L = \frac{0.20}{0.30} \cdot 2 \text{ mm} = 1.4 \text{ mm}$$

$$\text{Source 2: } Sr = 0.43 \quad (27)$$

$$L = \frac{0.20}{0.43} \cdot 2 \text{ mm} = 0.9 \text{ mm}$$

These values correspond roughly to the length scales of the sliders of the pantograph model. The single slider elements have a thickness of 1.9 mm, the outer curved elements (“pantograph horn”), however, are only 1.0 mm thick. These elements have a different orientation to the flow and to the array microphones, please refer to the photograph in Fig. 4. Since the radiation characteristics of the two regarded pantograph elements is similar to a classical cylinder in cross flow, the horn radiates also in lateral direction, where the array microphones are situated. The dipole at the sliders has,

however, only a vertical component, and the array microphones receive mainly reflections on the curved surface of the train’s roof. This might be the reason, why the beamforming maps depicted in Fig. 14 and in Fig. 15 provide a reasonable source location for source 2, but a unphysical one for source 1.

In the next step the influence of the flow velocity influence on the Strouhal number is discussed. As shown in Fig. 13(b), a flow velocity dependent shift of the peak Strouhal numbers can be observed. The peak Strouhal numbers for the two discussed sound sources versus the Mach numbers are illustrated in Fig. 17(a). There is only a weak influence of the Mach- and Reynolds number on the Strouhal number, and all relative fluctuations of the peak Strouhal number are less than 5%. The Strouhal number of the fundamental frequency (“x” - markers) as well as of the first higher harmonic (“o” - markers) of the sound emitted by source 2 (red lines) increases slightly with the Mach number. For source 1 a different trend is found. As mentioned before, the regarded sound sources seem to require a minimum Mach number, and thus the measurements for the lowest Mach number of $M = 0.058$ differ in some cases.

In the next step the power law between the emitted narrowband peak level and the Mach number is discussed. Neglecting Reynolds number dependent effects, one expects a relation for a cylinder in cross flow for the acoustic power, which is proportional to the 6th power of the Mach number, but also of the 2nd power of the Strouhal number (see Eq. (8) in Sec. 2.2.1). The same relation is assumed now for the pantograph. To estimate the power law exponent m based on a linear fit, the data are considered as follows to take the Strouhal number dependence into account:

$$\log p'^2 - 2 \log S \propto m \log M. \quad (28)$$

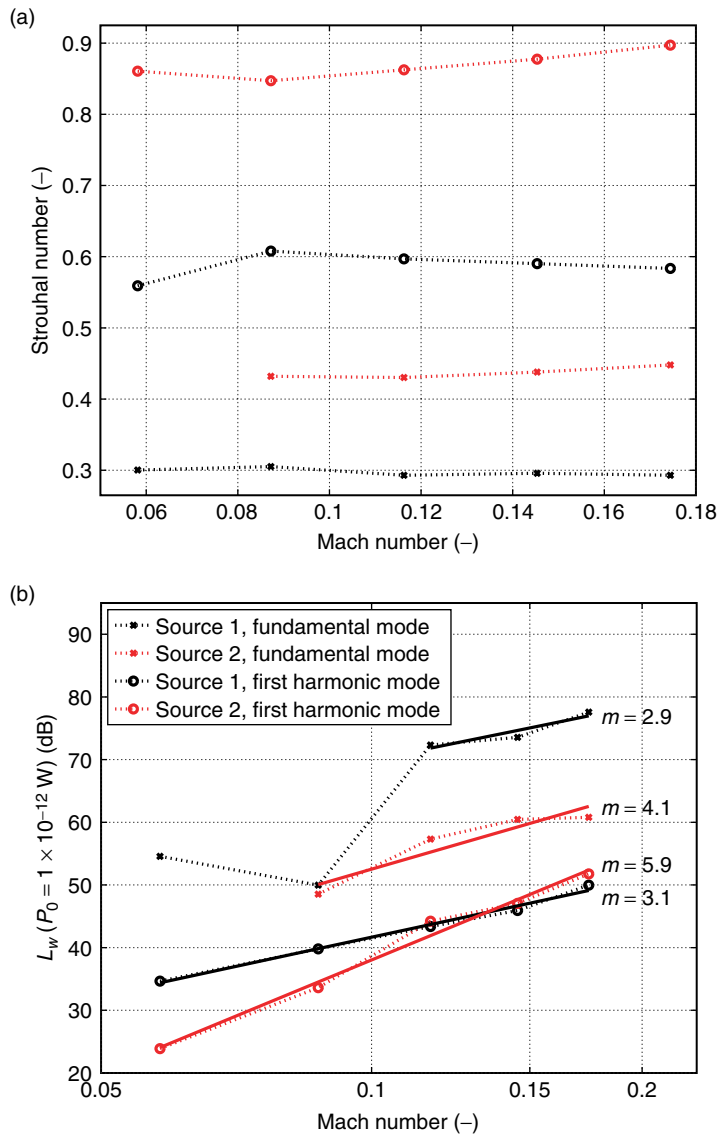


Figure 17: (a): The Mach - and Reynolds number dependence of the Strouhal number. (b): The relation between Mach number and the peak sound power level, for the four discussed peak frequencies (see legend in graph 17(a)).

Finally, the data are processed in terms of the sound power levels:

$$L_w - 20 \log Sr \propto m \log M. \quad (29)$$

Fig. 17(b) shows the peak sound power levels at different Mach numbers between $0.058 < M < 0.175$ for sources 1 (black lines) and source 2 (red lines). The data are based on the beamforming spectra, shown in Fig. 13. The solid lines represent the linear regression fit. For source 1 (horn) a rather small power exponent of $m = 2.9$ of the fundamental mode, and $m = 3.1$ of the first higher harmonic is obtained. Especially for the

fundamental mode the data are not consistent for all Mach numbers, and accordingly, only the data of the measurements at Mach numbers $M \geq 0.086$ are used for the calculation. For source 2 (slider elements) the lowest Mach number has been neglected. For this source the power exponent is $m = 4.1$ for the fundamental mode, and $m = 5.9$ for the higher harmonic. The data reveal significant deviations from the expected trend lines in some cases, and the results for the calculated power law exponents must be interpreted with caution. The aforesaid combination of the directional pattern of the sources

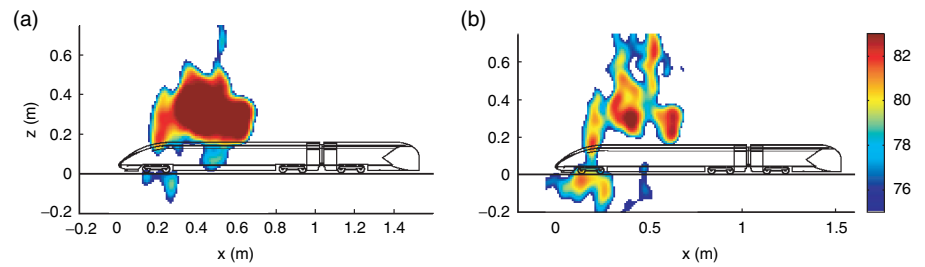


Figure 18: 4 kHz one-third octave source maps of the ICE 3, measured in the DNW-KKK at $U_\infty = 72$ m/s, using the Delay and Sum Beamforming algorithm, the Sound power levels are colour-coded; with reference power $P_0 = 1 \times 10^{-12}$ W. (a): When using the standard method a strong artificial source appears above the train's head. (b): Additional application of the BiClean algorithm to the data attenuates the strength of the artificial source and improves the signal-to-noise ratio.

and reflections seem to influence not only the source position, but also the measured source strength. To get more accurate results more details of the source characteristic are needed.

4.2. MEASUREMENT AT HIGHER REYNOLDS NUMBERS IN THE CRYOGENIC WIND TUNNEL (DNW-KKK)

This section describes the experiments conducted in the cryogenic wind tunnel DNW-KKK on the ICE 3 without pantograph at Mach numbers between $0.100 < M < 0.300$ and Reynolds number between $0.450 \times 10^6 < Re < 3.567 \times 10^6$.

The measurements reveal a high background noise level inside the test section: The closed test section with hard walls causes a reverberant environment. Furthermore, it turns out that the used ground board produces more self noise compared to the splitter plate used in the aeroacoustic wind tunnel, because all the mountings underneath the plate are exposed to the flow. A more detailed analysis has shown, that the ground board acts as a spatially expanded coherent sound source, leading to a strong spot in the source maps as shown in Fig. 18(a). The latter limits the quality of the beamforming results. In order to improve the results, the BiClean algorithm (introduced in Sec. 3.2) is

applied to the data, whereby the strength of the spot can be reduced, as depicted in Fig. 18(b). The noise of the splitter plate seems to de-correlate the array signals, and therefore applying BiClean can increase the source levels outside the spot by up to 3 dB. For all results discussed below the BiClean algorithm was used for the calculation of a “cleaned” cross correlation matrix R , and again CLEAN-SC for the final beamforming evaluation. Nevertheless, the signal-to-noise ratio of the measurements under these difficult conditions is restricted, and therefore the results are discussed in terms of one-third octave bands. Fig. 19 depicts source maps of the ICE 3 for one-third octave bands between 3.15 kHz and 10 kHz, measured at $M = 0.25$ ($U_\infty = 72.2$ m/s) and $T = 200$ K, presented over 8 dB dynamic range. In comparison to the results obtained in the aeroacoustic wind tunnel, discussed in the previous Sec. 4.1, the current maps indicate a higher noise level and the sound source at the first bogie cannot be identified unambiguously in all frequency bands. Thus, the below discussed integrated spectra exhibit more noise. Acoustic reflections on the ground board occur and the source position of the first bogie is shifted downwards. The integration area is large enough to account for this effect, and is identical to the one used for the study in the aeroacoustic wind

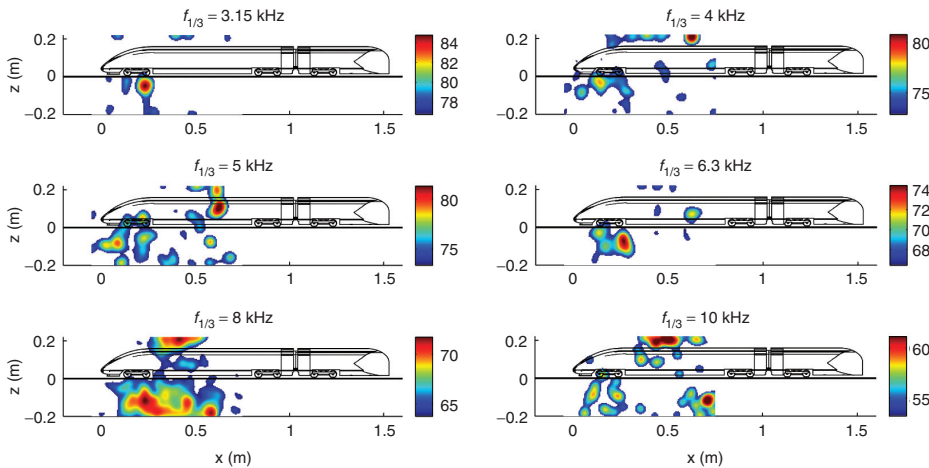


Figure 19: One-third octave source maps of the ICE 3, measured in the DNW-KKK at $M = 0.25$ ($U_\infty = 72.2$ m/s) and $T = 200$ K. Sound power level is colour-coded over 8 dB dynamic range; with reference power $P_0 = 1 \times 10^{-12}$ W.

tunnel, given in Fig. 10, left.

Fig. 20(a) and Fig. 20(b) show spectra of the first bogie for the aforesaid Mach numbers, measured at two different temperatures $T = 200$ K and $T = 100$ K, corresponding to a Reynolds number range of $0.450 \times 10^6 < Re < 1.351 \times 10^6$ for $T = 200$ K, and $1.198 \times 10^6 < Re < 3.567 \times 10^6$ for $T = 100$ K. All spectra are discussed in terms of the Helmholtz number He , Eq. (15). For both Reynolds number ranges, we obtain similar dependencies of the sound power level spectra on the Mach number. Within the measuring accuracy, the sound power levels and the shape of the spectra are comparable between the two temperatures. Furthermore, the shape of the spectra does not show a Mach number dependence³ - qualitatively this is in agreement with results of the measurements at lower Reynolds numbers in the aeroacoustic wind tunnel. Due to the limited signal-to-noise ratio in such an acoustically optimised wind tunnel described above, these measurements do not allow a narrowband representation of the spectra, and so, the characteristic peaks, which have been identified before in Fig. 11(a), can not be recovered here.

As depicted in Fig. 20(c), the exponent of the overall power law is again nearly $m = 6$ for the measurements conducted at temperatures between $T = 100$ K and $T = 200$ K. This corresponds to a Reynolds number range between $Re = 0.45 \times 10^6$ and $Re = 3.58 \times 10^6$.

The discussion of the spectra presented in Fig. 20(d), measured for a constant Mach number of $M = 0.2$ and different Reynolds numbers in the range of $0.903 \times 10^6 < Re < 2.375 \times 10^6$ focuses on the Reynolds number dependence of the aeroacoustics of the first bogie. Here, a variation of the Reynolds number is obtained by variation of the temperature of the fluid. The spectra reveal only a weak Reynolds number dependence; since, within the measuring accuracy, the spectra lie on top of each other. The differences in the order of magnitude ± 3 dB can be explained by uncertainties due to the restricted signal-to-noise ratio of the measurements. Clear tendencies of the relationship between sound power level and Reynolds number cannot be identified.

4.3. COMPARISON OF THE RESULTS OF THE AWB AND THE DNW-KKK

In this section the data acquired at the two wind tunnels are compared. The

³Except the measurement at $M = 0.15$; at this Mach number a temperature independent background noise mechanism was active, which influenced the results.

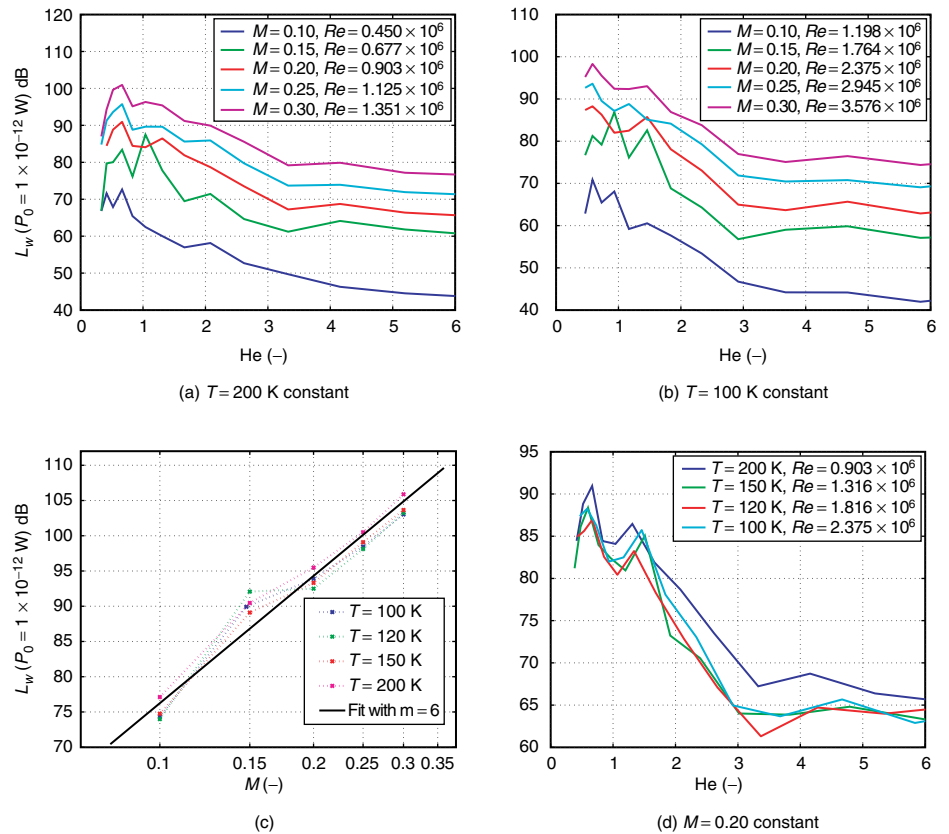


Figure 20: (a): Spectra of the first bogie, measured in the cryogenic wind tunnel for different Mach numbers and a constant temperature of $T = 200$ K. (b): As shown in (a), but for a temperature of $T = 100$ K. (c): Temperature dependence of the relation between Mach number and the overall sound power level. (d): Spectra for different Reynolds numbers at constant Mach number $M = 0.2$.

results of the first bogie for the Mach number interval $0.10 < M < 0.20$ of both wind tunnels are depicted in Fig. 21. The Mach number nearly the same for both cases. The solid lines reflect spectra measured in the AWB and the dashed lines those measured in the KKK-DNW. The Reynolds numbers differ, because the data of the DNW-KKK are not available for a temperature of $T = 290$ K, at which the experiments in the AWB were conducted. Therefore, here the presented DNW-KKK measurements have been done at $T = 200$ K. As shown in the previous section, the Reynolds number has no significant effect on the acoustics of the first bogie, and so the comparison is valid.

Furthermore, two different kinds of microphone arrays have been used for the measurements. In the aeroacoustic

wind tunnel the microphones are calibrated under free-field conditions, and in the cryogenic wind tunnel the microphone membranes are installed behind a small cone in the array - fairing, and so they are calibrated under pressure field conditions. Hence, it is necessary to take the amplification of the amplitudes by a factor of two for the pressure field microphones into account. Expressed in terms of the logarithmic Decibel scale, it means, that one has to add

$$\Delta_{spI} = 20 \log \frac{A_{pf}}{A_{ff}} = 20 \log 2 \approx 6 \text{ dB} \quad (30)$$

to the spectra, estimated with the array of free-field microphones. Thereby A_{ff} denotes the amplitude under free-field conditions, and A_{pf} the amplitude under

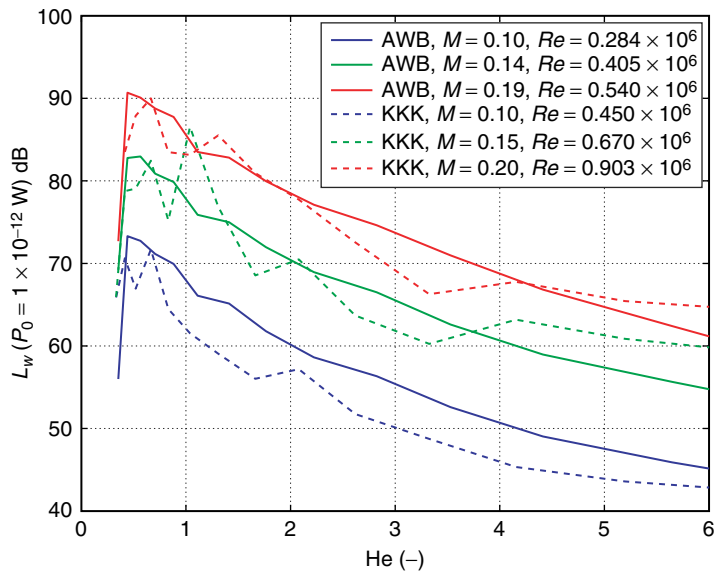


Figure 21: Comparison of spectra, measured in the AWB and in the DNW-KKK.

pressure-field conditions. Regarding the amplitude doubling, one obtains maximum sound power levels, which are in same order of magnitude in both cases. The one-third octave spectra do not reveal a Mach number dependence on the overall shape, which indicates that cavity mode excitation takes place at the bogie section in both wind tunnel setups. For higher frequencies the spectra measured in the cryogenic wind tunnel always lie above the spectra, measured in the aeroacoustic wind tunnel. This might be due to the fact, that at higher frequencies the bogie does not emit sound very effectively. The impact of the background noise increases, and the spectra contain more noise.

The overall power law exponents, estimated in Sec. 4.1 and Sec. 4.2, are in a quite good agreement with $m = 6.5$ (AWB) and $m = 6.0$ (DNW-KKK). Further, a quantitative comparison is difficult due to some major differences in the two setups. The aeroacoustic wind tunnel has an open test section, and the microphones are installed outside the flow. As a consequence, the sound has to propagate through the wind tunnel's turbulent layer. This leads to a coherence loss between the microphone signals which finally decreases the sound power levels. This

effect intensifies with increasing Mach number, and moreover, is frequency dependent: Experimental studies in the AWB from Kröber et al. [43] have shown, that this effect becomes dominant for frequencies higher than $f = 20$ kHz, which corresponds to a Helmholtz number (Eq. (15)) of $He = 7$. This effect, which causes deviations of up to 3 dB in the the regarded frequency range, is not considered here.

Although a direct comparison of the results of both measurements similar tendencies are obtained from both studies.

5. CONCLUSIONS

Two different sources of sound with different characteristics are identified in the aeroacoustic wind tunnel: the aeroacoustic noise from the bogie section is dominant for frequencies $f < 5$ kHz and can be characterised by cavity mode excitation. The overall shape does not change significantly within the investigated Mach number range. Two velocity-independent humps have been identified in the spectra. A characteristic dimension of the bogie section of the train model, which is in the order of centimetres, is probably responsible for the observed tonal contributions. The power law exponent

for the peaks and the overall sound power level is around $m = 6.6$. The pantograph is the dominant sound source for frequencies higher than $f = 5$ kHz. It is a strong tonal source and the frequency peaks reveal a nearly linear Mach number dependence. Further, several peaks with constant Strouhal numbers including their higher harmonics can be identified in the spectra. It can be assumed, that the sound source has a strong directivity. The peaks in the spectra can be assigned to the slider elements and to the horn of the pantograph. It is found, that the beamforming technique can fail to determine the correct source location and strength due to the source characteristic and possible reflections on the roof of the train. Therefore, also the calculation of the power law exponent discloses inconsistencies, which are attributed to the aforesaid source properties. The power law exponents of the sources of the pantograph vary between $2.9 < m < 5.9$.

In order to obtain higher Reynolds numbers a second measurement in the cryogenic wind tunnel was conducted. For this measurement the same model without pantograph was used. To assure a comparability of aeroacoustic measurements conducted at different temperatures, the Helmholtz number as nondimensional frequency is used. The experiments show only a weak Reynolds number dependence of the noise of the first bogie. The Mach number dependence is similar to what has been found in the previous experiments in the aeroacoustic wind tunnel. The power law exponent again is nearly $m = 6$ over a wide Reynolds number range. A comparison of the two measurements in the different wind tunnels discloses the same tendencies in the acoustic spectra of the first bogie.

REFERENCES

- [1] Barsikow B., King III W.F., and Pfizenmaier E. Prognosen zum Lärmpegel des R/S-VD für die Maximalgeschwindigkeit 350 km/h. *DFVLR-IB 22214-81/2*, 1981. DFVLR, Abteilung Turbulenzforschung, Berlin.
- [2] Mellet C., Letourneaux F., Poisson F., and Talotte C. High speed train noise emission: Latest investigation of the aerodynamic/rolling noise contribution. *Journal of Sound and Vibration*, 293(3–5): 535–546, June 2006. Proceedings of the Eighth International Workshop on Railway Noise.
- [3] Pfizenmaier E., Barsikow B., Bechert D., and King III W.F. Rad/Schiene-Lärm und Aeroakustik schneller Eisenbahnzüge. *DFVLR-IB 22214-82/45*, 1985. DFVLR, Abteilung Turbulenzforschung, Berlin.
- [4] Dittrich A.G. and de Beer F.G. The Applicability of prEn ISO 3095 for European Legislation on Railway Noise, Final Draft v3.2. *TNO-report HAG-RPT-010014*, February 2001.
- [5] Barsikow B., King III W.F., and Pfizenmaier E. Wheel/rail noise generated by a high-speed train investigated with a line array of microphones. *Journal of Sound and Vibration* 118(1), 99–122, 1987.
- [6] Martens A., Wedemann J., Meunier N., and Leclere A. High speed train noise - sound source localization at fast passing trains. *Deutsche Bahn AG, Sociedad Espanola de Acustica, S.E.A.*, 2009.
- [7] Yamazaki N., Takaishi T., Toyooka M., Nagakura K., Sagawa A., and Yano H. Wind tunnel tests on the control of aeroacoustic noise from high speed train. *9th International Workshop on Railway Noise, Munich*, 2007.
- [8] Dassen T., Sijtsma P., and van Haaren R. The Noise of a High-Speed Train Pantograph as measured in the German-Dutch Wind Tunnel DNW. *2nd International Workshop on the AeroAcoustics of High-Speed Trains (AAT)*, Berlin, 1997.
- [9] Barsikow B. and Klemenz M. Pantograph Noise - A Sound Source Relevant to High-Speed Trains? *The International EAA/EEAA*

- Symposium Transport and Vibration, Tallinn, 1998.*
- Royal Society, London, A, 231(1187): 505–514, 1955.
- [10] Pfizenmaier E., King III W.F., Schewe G., and Herrmann I. Wind-kanaluntersuchungen an einem Stromabnehmer für den Intercity-Experimental (ICE) der Deutschen Bundesbahn. *DFVLR-IB 22214-85/B5*, 1985. DFVLR, Abteilung Turbulenzforschung, Berlin.
- [11] King III W.F., Pfizenmaier E., and Herrmann I. Schallquellen an Hochgeschwindigkeitsstromabnehmern und Möglichkeiten zur Reduktion. Eine Literaturübersicht. *DFVLR-IB 92517-97/B1*, 1997. DFVLR, Institut für Antriebstechnik, Abteilung Turbulenzforschung, Berlin.
- [12] Goodyer M.J. and Kilgore R.A. High-Reynolds number cryogenic wind tunnel. *American Institute of Aeronautics and Astronautics*, 11(5), 1973.
- [13] Ehrenfried K. *Strömungsakustik*. Berliner Hochschulschriften, Mensch & Buch Verlag, 2004.
- [14] Sutherland W. The viscosity of gases and molecular force. *Philosophical Magazine Series 5*, pages 507–529, 1893.
- [15] Hilsenrath J., Beckett C.W., Benedict W.S., Fano L., Hoge H.J., Masi J.F., R.L. Nutal, and Touloukian Y.S. *Tables of Thermodynamik and Transport Properties*. Pergamon Press, 1960.
- [16] Strouhal V. Über eine besondere Art der Tonerregung. *Annalen der Physik*, 241(10): 261–251, 1878.
- [17] Ahlefeldt T. and Koop L. Microphone array measurements in a cryogenic wind tunnel. *15th AIAA/CEAS Aeroacoustics Conference, Miami, FL, USA*, (AIAA 2009–3185), 2009.
- [18] Lighthill M.J. On sound generated aerodynamically, I. General Theory. *Proceedings of the Royal Society, London, A.*, 211(1107): 564–587, 1952.
- [19] Curle N. The influence of solid boundaries upon aerodynamic sound. *Proceedings of the*
- [20] Phillips O.M. The intensity of aeolian tones. *Journal of Fluid Mechanics*, 1: 607–624, 1956.
- [21] Tam C.K.W. and Block P.J.W. On the tones and pressure oscillations induced by flow over rectangular cavities. *Journal of Fluid Mechanics*, 89(2): 373–399, 1978.
- [22] Roshko A. Some measurements of flow in a rectangular cutout. Technical Report TN 3488, NACA, 1955.
- [23] Rossiter J.E. Wind-tunnel experiments on the flow over rectangular cavities at subsonic and transonic speeds. *Reports and memoranda (Aeronautical Research Council, Great Britain)*, 3438, 1967.
- [24] Plumblee H.E., Gibson J.S., and Lassiter L.W. A theoretical and experimental investigation of the acoustic response of cavities in an aerodynamic flow. Technical Report WADD-TR-61-75, U.S. Airforce, 1962.
- [25] East L.F. Aerodynamically induced resonance in rectangular cavities. *Journal of Sound and Vibration*, 3:277–287, 1966.
- [26] Block P.J.W. and Heller H. Measurements of farfield sound generation from a flow-excited cavity. Technical Report TM X-3292, NASA, 1975.
- [27] Pott-Pollenske M. and Delfs J. Enhanced Capabilities of the Aeroacoustic Wind Tunnel Braunschweig. *14th AIAA/CEAS Aeroacoustics Conference, Vancouver, BC, Canada*, (AIAA-2008-2910), 2008.
- [28] Jönsson M. and Loose S. Experimental investigation of the flow field underneath a generic high-speed train and the effects of ground and train roughness. In *Aerodynamics of Heavy Vehicles III: Trucks, Busses and Trains, Potsdam, Germany*, 2010. Under review.
- [29] Grunwald K.J. Aerodynamic characteristics of vehicle bodies at cross-wind conditions in

- ground proximity. *NASA TN D-5935*, 1970.
- [30]Katz J. *New Directions in Race Car Aerodynamics*. Bentley Publishers, 2nd edition edition, 2009.
- [31]Schlichting H. and Gersten K. *Boundary Layer Theory*. Springer, 8. edition, 2000.
- [32]Johnson D.H. and Dudgeon D.E. *Array Signal Processing: Concepts and Techniques*. Prentice-Hall, Englewood Cliffs, NJ, 1993.
- [33]Mueller T.J., editor. *Aeroacoustic Measurements*. Springer Verlag, 2002.
- [34] Sijtsma P. CLEAN Based on Spatial Source Coherence. *International Journal of Aeroacoustics*, 6:357–374, 2007.
- [35]Ehrenfried K., Koop L., Henning A., and Käpernick K. Effects of Wind-Tunnel Noise on Array Measurements in Closed Test Sections. *BeBeC-2006-07*, 2006. ISBN 978-3-00-019998-1. 1st Berlin Beamforming Conference, 22–23 November, 2006.
- [36]Koop L. and Ehrenfried K. Microphone-array processing for wind-tunnel measurements with strong background noise. *14th AIAA/CEAS Aeroacoustics Conference, Vancouver, BC, Canada, (AIAA-2008-2907)*, 2008.
- [37]Lauterbach A., Ehrenfried K., Koop L., and Loose S. Procedure for the Accurate Phase Calibration of a Microphone Array. *15th AIAA/CEAS Aeroacoustics Conference, Miami, FL, USA, (AIAA 2009-3122)*, 2009.
- [38]Koop L. *Experimental Aeroacoustics*, chapter Beam Forming Methods in Microphone Array Measurements - Theory, Practice and Limitations, pages 1–78. Von Karman Institute for Fluid Dynamics, VKI LS 2007-01, ISBN 978-2-930389-70-2, 2007.
- [39]Amiet R.K. Refraction of sound by a shear layer. *Journal of Sound and Vibration*, 58(4):467–482, 1978.
- [40]Brooks T.F. and Humphreys M.W. Effect of Directional Array Size on the Measurement of Airframe Noise Components. *5th AIAA/CEAS Aeroacoustics Conference, Bellevue, USA, (AIAA-99-1958)*, 1999.
- [41]Ahuja K. K. and Mendoza J. Effects of Cavity Dimensions, Boundary Layer and Temperature on Cavity Noise With Emphasis on Benchmark Data To Validate Computational Aeroacoustic Codes. *NASA Contractor Report 4653*, 1995.
- [42]Liu Yu, Dowling A. P., and Quayle A.R. Numerical Simulation of Beamforming Correction for Dipole Source Identification. *BeBeC-2008-05, GfA, Gesellschaft zu Förderung angewandter Informatik e.V., Berlin*, 2008.
- [43]Kröber S., Ehrenfried K., Koop L., Lauterbach A., and Henning A. Systematic comparison of microphone array measurements in open and closed wind tunnels. *16th AIAA/CEAS Aeroacoustics Conference, Stockholm, Sweden, (AIAA-2010-3734)*, 2010.

\$65000 INSIDE 65 DB

Homes within the 65dB contour of Barnes Regional Airport (Westfield MA) are being sound proofed on a 9 year rolling programme. The average cost per house is approximately \$65000. 90% of the funding comes from the FAA, the remainder from the state and the city.